Semnan University

Journal of Modeling & Simulation in Electrical & Electronics Engineering (MSEEE)

Journal homepage: **https://mseee.semnan.ac.ir/**

ISSN: 2821-0786

Intelligent Fault Tolerant Procedure Design for Nonlinear Dynamics of Induction Furnace Systems: Adaptive Inverse Dynamics Approach

Reza Ghasemi*[1] and Alireza Borjali[1]

***Abstract*- This paper presents an adaptive inverse dynamic control (AIDC) designed as a fault-tolerant controller for nonlinear models of coreless induction furnace systems. Unlike other research focused on intelligent identification of nonlinear systems, this methodology developed an inverse intelligent process as a universal controller applicable to various nonlinear systems. In induction furnace operations, accurately tracking the target reference temperature is critical for maintaining the crystalline properties of metals; for instance, to produce iron ferrite with 12.22 wt% carbon, the temperature must be held at 912°C. The proposed AIDC approach features an online inverse model identifier, updated using the back-propagation (BP) algorithm. This involves three techniques: 1) multilayer perceptron (MLP), 2) adaptive neuro-fuzzy inference system (ANFIS), and 3) neural networks, all used to identify the system's inverse dynamics as a nonlinear controller. Key benefits of the AIDC include the convergence of faulty states to nominal conditions, robust system design, and reduced impact of faults on system performance. Simulation results demonstrate the effectiveness of this approach.**

***Index Terms:* Adaptive Inverse Control; Induction Furnace; Back-Propagation Algorithm; Neural Network; Multilayer Perceptron; Adaptive Neuro-Fuzzy Inference System.**

HIGHLIGHT:

- This approach deals with a nonlinear nonaffine dynamical model for the Induction Furnace system.
- Both the Neuro and ANFIS Fault-hiding methodologies are presented and developed in this tactic.
- The actuator fault should be hidden based on the proposed methods.
- Both the direct and inverse Neuro and ANFIS dynamical methodologies are improved in this strategy.

I. Introduction

The origins of induction furnaces date back to Michael Faraday and his achievements regarding the principle of electromagnetic induction. Far ahead, inventions and experiments were made in this field, such as De Ferranti in 1870 and Edward Allen Colby in 1890. Based on the research, induction furnaces are divided into the core and the coreless types [1]. Nowadays, the principles of induction heating are widely used in industrial and consumer applications such as melting, alloy making, and induction brazing [2]. The Basic principle of heat production by conduction has been understood and applied to manufacturing since 1920 [3]. The merits of the induction furnace over the fossil fuel furnace are better performance and efficiency, reliability, cleanness, and flexibility. Induction furnaces produce heat cleanly, without combustion, unlike fossil fuel furnaces. The coreless induction furnace is an energy-transfer device in which energy is transferred directly from the induction coil to the materials intended for melting. The melting process is done through the electromagnetic field generated by the induction coil [22].

Temperature control in induction furnaces has garnered significant research interest. Study [2] presents three temperature control modes: a linear model, a saturated linear model, and a saturated linear model with an anti-windup PI controller. In [4], an advanced temperature control strategy is investigated for an industrial box furnace by exploiting a

Received; 2025-12-08 Revised; 2026-02-22 Accepted; 2026-02-28

1. Department of Electrical Engineering, University of Qom, Qom, Iran.
*Corresponding author: r.ghasemi@qom.ac.ir

Cite this article as:
Ghasemi, A. and Borjali, A, R. (2026). Intelligent Fault Tolerant Procedure Design for Nonlinear Dynamics of Induction Furnace Systems: Adaptive Inverse Dynamics Approach. *Journal of Modeling & Simulation in Electrical & Electronics Engineering (MSEEE)*. Semnan University Press. 6 (2), 43-53.
DOI: https://doi.org/10.22075/MSEEE.2026.39990.1240

physics-based thermodynamic model available at the early design stage. The study compares conventional PID control with model predictive control (MPC) and virtual reference feedback tuning (VRFT). Research in [5], Hu et al. present a nonlinear dynamic modeling and control framework for large-scale reheating furnaces based on a zone-method radiation model integrated with a self-adapting predictive control scheme. The proposed approach accurately captures transient furnace dynamics under highly variable operating conditions, including non-uniform batch scheduling and production delays, achieving discharge temperature prediction errors within ±10 °C. In [6], a fuzzy controller is implemented in an induction furnace with an analog inverter, aiming to maintain a uniform heating temperature of 450°C for aluminum bars within the induction coil. Study [7] develops a 2-degree-of-freedom model-based temperature controller for an induction-heating system that processes thin metal strips using a simplified finite-element model. Finally, in [8], this paper systematically analyzes the application of FOPID controllers in various temperature-regulated systems, including bioreactors, induction heating, and medical environments, demonstrating superior performance compared to conventional PID controllers in terms of stability, response speed, and disturbance rejection. The study also highlights practical tuning approaches and the industrial feasibility of FOPID controllers for modern thermal control systems. In [9], A distributed adaptive control framework is proposed for temperature regulation in multi-zone HVAC systems, explicitly accounting for thermal interactions between neighboring zones and time-varying uncertainties. By incorporating online parameter estimation and inter-zone information exchange, the proposed scheme achieves robust temperature tracking without requiring accurate system models. [10] Zuo et al. propose an improved decoupling control strategy for a multivariable gas heating furnace characterized by strong coupling, nonlinear dynamics, time delays, and parameter uncertainties. By combining a decoupling network based on the small-gain theorem and frequency-domain function approximation with IMC-based PID controllers, the system is effectively transformed into independent single-loop subsystems. In [11], A modified speed-optimal temperature control algorithm is proposed for electric resistance furnaces used in metal heat treatment, aiming to minimize heating time while limiting temperature overshoot. Stojanovski and Stankovski present a comprehensive comparison of several predictive control strategies, including linear MPC, multiple-model MPC, hybrid MPC, and hybrid multiple-model MPC, for a high-consumption industrial gas-fired furnace in [12].

In [13], an adaptive neural network scheme is developed for nonlinear time-varying systems with changing parameters. [14] describes a fuzzy adaptive tracking approach for stochastic-constrained nonlinear systems utilizing stochastic barrier Lyapunov functions. [15] introduces a passive inverse dynamic fault-tolerant control (FTC) and an adaptive principal component analysis (PCA) algorithm for data processing. The processed data is then trained with an MLP neural network and an adaptive BP algorithm to minimize tracking errors based on PCA-uncorrelated measurements. A nonlinear autoregressive neural network with exogenous inputs (NARX) is employed as an inverse dynamical system to optimize photovoltaic power tracking [16]. [17] introduces an adaptive inverse control (AIC) system for vehicle path tracking, comprising two key components: a model identifier and an inverse model controller, with a back-propagation algorithm for parameter updates. Study [18] compares a conventional neural model with a modified neural network trained using the BP algorithm. Research in [19] introduces an optimized neural network inverse approach for quad-rotors, with retraining based on new maneuver data. In [20], an adaptive inverse controller is proposed for unmanned aerial vehicles, leveraging a predetermined reference position. Finally, in [21], an optimal inverse controller for the dynamical fuzzy neural network of tunneling shield machines is presented.

Temperature control is essential in metal melting processes to preserve the chemical composition and structural integrity of molten metal foam, particularly in induction furnaces characterized by strong nonlinear dynamics and uncertainties. The induction furnace exhibits nonlinear dynamics with time-varying parameters, complicating model and controller development. Neural network systems can effectively address these challenges, particularly in inverse modeling and control [1].

The main scientific objective of this paper is to develop a fault-tolerant temperature control mechanism capable of maintaining accurate tracking performance in the presence of faults. Unlike conventional fault-tolerant control methods such as Model Predictive Control (MPC) or Sliding Mode Control (SMC), which often require precise system models or suffer from chattering phenomena, the proposed approach eliminates the need for explicit fault detection and isolation modules. To achieve this goal, an adaptive inverse control framework based on ANFIS and MLP neural networks is employed to regulate the furnace temperature at a target value of 912 °C. For the inverse scenario, the neural network learns from the outputs, output delays, and input delays provided as inputs. The proposed fault-tolerant inverse structure effectively compensates for fault-induced performance degradation, significantly reducing overshoot, rise time, and tracking error. Simulation results confirm that the tracking error converges close to zero even under fault conditions, demonstrating that the novel contribution of this work lies in embedding fault tolerance within the adaptive inverse control structure rather than merely applying intelligent controllers to the induction furnace.

The remainder of the paper is structured as follows: the second section presents the Nonlinear Coreless Induction Furnace Dynamical Model, while the third discusses the design and modeling of the adaptive MLP inverse controller. The fourth section details the design and modeling of the adaptive inverse controller using the ANFIS network. The fifth segment examines the simulation results, and the final section concludes the paper.

II. NONLINEAR DYNAMICAL MODEL OF CORELESS INDUCTION FURNACE

This approach utilizes a core-less induction furnace for electric heating to enhance performance, efficiency, reliability, cleanliness, and flexibility in the metal industry. As illustrated in Fig. 1, the induction furnace consists of a copper coil, a tubular shell, a cooling system, and tilting capabilities [3].

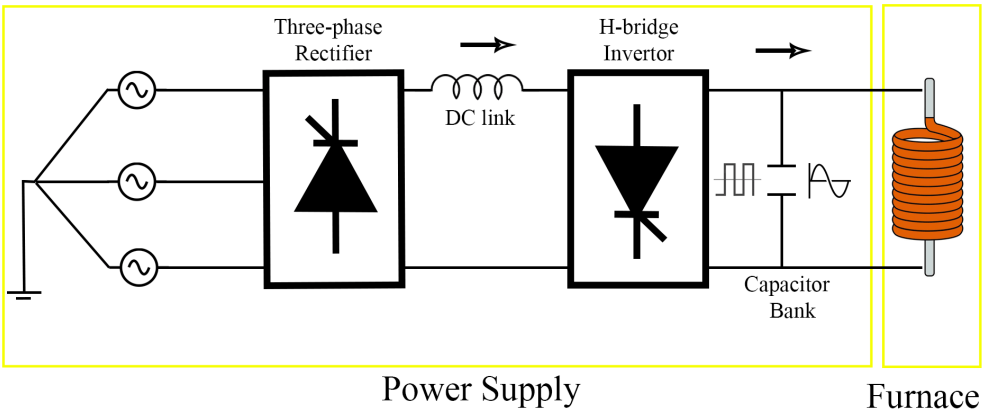

Fig. 1. The Main Components of Coreless Induction Furnaces [3]

The power supply, which consists of 1) an AC to DC rectifier, 2) a DC-link, 3) a DC-to-AC inverter, and 4) capacitor banks, generates the power of the mentioned system [3]. The induction furnace model includes the electrical and thermal dynamical subsystems.

A. Electrical System Dynamics

The electrical system dynamics of the induction furnace can be modeled as an equivalent electrical circuit, as illustrated in Fig. 2. The electric section consists of three sections [3]:

1. The equivalent circuit of an induction furnace (RET)
2. Parallel resonant circuit (RSP)
3. The current fed inverter (FCI)

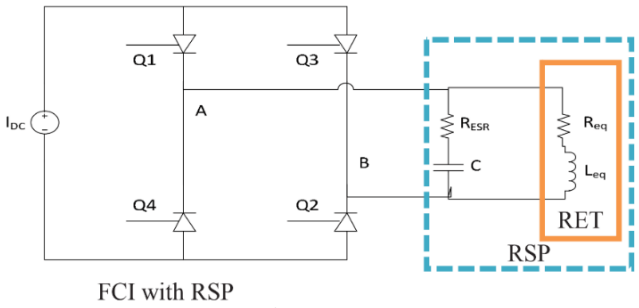

Fig. 2. The Equivalent Circuit of the Induction Furnace [3]

The furnace is designed such that the induced current is transformed into thermal energy capable of melting the raw material. Accordingly, the induction furnace can be modeled by an equivalent electrical circuit composed of an equivalent resistance connected in series with an equivalent inductance [3].

The equivalent resistance R_{eq} represents the combined effect of the coil resistance R_{coil} and the shunt resistance R_{ch}, and can be expressed by (1) as follows [3]:

$$R_{eq} = R_{coil} + R_{ch} \tag{1}$$

The coil resistance is defined as the product of the coil resistivity ρ_c and the coil length l_c, divided by the coil cross-sectional area $A_c = \pi x^2$. Where $x = \frac{d_m}{2}$, which can be expressed in (2) as follows [3]:

$$\begin{cases} l_c = \pi D_{in} N \\ R_{coil} = \dfrac{\rho_c l_c}{A_c} \end{cases} \tag{2}$$

The shunt resistance represents the resistance associated with mutual inductance effects, where the square of the number of windings is multiplied by the load resistance, corresponding to the resistance of the raw material to be melted (R_L). This relationship is expressed by (3) as follows [3]:

$$R_{ch} = \frac{\rho_m l_m}{A_m} \tag{3}$$

where the electrical resistivity of iron ρ_m is 2.83×10^{-8}, and ($l_m = 2\pi x$) denotes the length of the tube cross section, which is defined as half of the distance along the vertical axis. Sectional area of the tube (A_m) is [3]:

$$\begin{cases} A_m = H_m dx \\ dx = d_o = \sqrt{\dfrac{\rho_m}{\pi \mu f}} \end{cases} \tag{4}$$

The equivalent inductance corresponds to the total self-inductance reduced by the effect of mutual inductance, and can be represented by (5) as follows [3]:

$$L_{eq} = L_1 - NL_M \frac{\mu N^2 \pi D_{in}^2}{4H_{in}} - \frac{\sqrt{2} I_m R_{ch} \mu}{B_m H_{in} 2\pi f} \tag{5}$$

The system can be configured using the impedance of a series capacitor bank, $Z_1 = R_{ESR} + \frac{1}{sC}$, together with the furnace circuit impedance, $Z_2 = R_{eq} + sL_{eq}$, such that the overall impedance (Z_T), output voltage of the inverter (V_s) and coil current (I_{coil}) are expressed in (6) [3]:

$$\begin{cases} Z_T = \dfrac{Z_1 Z_2}{Z_1 + Z_2} \\ V_s = Z_T I_s \\ I_{coil} = \dfrac{V_s}{Z_2} \end{cases} \tag{6}$$

An inverter with a constant current input, also known as a current-fed inverter, operates as a PWM-based switching device that regulates the coil current. The PWM signal is generated through the comparison of a sinusoidal reference signal (V_{ref}) with a triangular carrier signal (V_{tri}). Assuming a constant DC input voltage, the inverter output voltage is

controlled by adjusting the modulation gain of the PWM signal. where the PWM signal gain and the corresponding inverter output voltage are given as [3]:

$$\begin{cases} K_{PWM} = \dfrac{V_{dc}}{V_{tri}} \\ V_s = K_{PWM} V_{ref} \end{cases} \tag{7}$$

The input power of the induction furnace can be regulated by adjusting the amplitude of the reference voltage (V_{ref}). The reference voltage is determined by the controller output signal (V_{CON}) and subsequently scaled through a reference voltage signal generator with gain (K_G) [3].

$$V_{ref} = K_G V_{CON} \tag{8}$$

Meanwhile, I_{eff} denotes the effective coil current. The coil current (I_{coil}) can be determined in differential form as follows [3]:

$$K_{PWM} K_G V_{ref} = L_{eq} \frac{d(I_{coil})}{dt} + R_{eq} I_{coil} \tag{9}$$

B. Thermal System Dynamics

The Dynamics of the thermal System represents the equilibrium thermal energy principle, which occurs during induction heating process [3]. The basic principle of energy balance can be expressed by (10):

$$heat\ input = heat\ output + heatloss \tag{10}$$

Based on the equation provided in [3]:

$$I_{coil}{}^2 K_R - d = mc \frac{d\theta}{dt} + J_1 \theta \tag{11}$$

C. Dynamics model of Induction Furnace System

According to [3], the state equation can be defined as follows:

$$\begin{bmatrix} \dot{x}_1 \\ \dot{x}_2 \end{bmatrix} = \begin{bmatrix} -\frac{J_1}{m.c} x_1 + \frac{K_R}{m.c} x_2^2 \\ -\frac{R_{eq}}{L_{eq}} x_2 \end{bmatrix} + \begin{bmatrix} 0 \\ \frac{K_{PWM}\, K_G}{L_{eq}} \end{bmatrix} u + \begin{bmatrix} -\frac{1}{m.c} \\ 0 \end{bmatrix} d \tag{12}$$

Where the state variables x_1 is the temperature of the induction furnace, x_2 stands for the coil current, u is the input of the system, and furthermore K_R and J_1 are expressed as follows:

$$\begin{cases} K_R = (\frac{1}{2} R_{eq} - R_{coil}) \\ J_1 = \frac{1}{R_T} \end{cases} \tag{13}$$

where m is the value of the mass; c is the specific heat capacity, R_{eq} stands for equivalent resistance, L_{eq} shows equivalent inductance, K_{PWM} depicts the signal gain of pulse width modulation, K_G refers to the gain reference voltage signal generator, d, R_T denote the disturbance and thermal resistance, respectively.

III. ADAPTIVE INVERSE MLP CONTROLLER

A. The Structure of AIC System

The main idea of adaptive inverse control (AIC) is to employ an inverse model as a controller to drive the plant output toward the desired reference signal [1]. To ensure accurate tracking performance, a neural network trained using the back-propagation (BP) algorithm is employed as an inverse model identifier. This inverse model is connected in series with the plant, forming an approximate identity mapping between the reference input and the system output.

The inputs of the inverse model identifier (IMI) consist of the plant input and output signals, along with their delayed versions. To enhance robustness against faults and external disturbances, an adaptive back-propagation (BP) learning scheme is employed to update the neural network weights of the IMI online, as illustrated in Fig. 3. The updated weights are then directly utilized in the inverse model controller.

Hence, this AIC system can accurately track the desired reference trajectory during the faults and external disturbances.

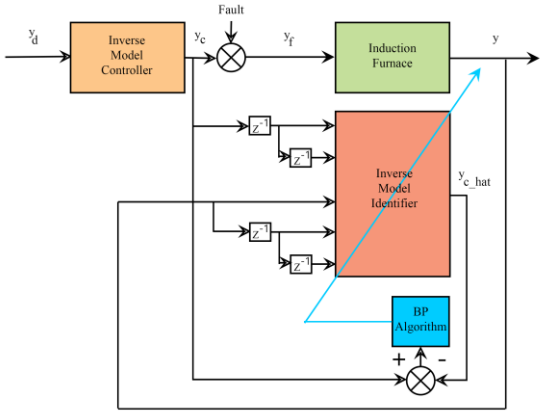

Fig. 3. The AIDC system for the induction furnace.

B. Online Modeling Using MLP & ANFIS Neural Network

Neural networks, as universal approximators, can accurately model complex nonlinear systems. In this study, both the multilayer perceptron (MLP) and the adaptive neuro-fuzzy inference system (ANFIS) are employed to model the dynamics of the proposed system.

1) MLP Algorithm structure

The structure of the MLP neural network is shown in Fig. 4, which consists of one input layer, one hidden layer, and one output layer. U, O and Y as the input vector, the hidden layer neuron vector, and the output vector, respectively, are expressed as below:

$$\begin{cases} U = [u_1\ u_2\ \cdots\ u_i\ \cdots\ u_n]^T, i = 1,2,\cdots,n \\ O = [o_1\ o_2\ \cdots\ o_j\ \cdots\ o_m]^T, j = 1,2,\cdots,m \\ Y = [y] \end{cases} \tag{14}$$

where n and m are the numbers of nodes in the input and hidden layers, respectively. Each one of u_i denotes the i^{th} input and o_j denotes the j^{th} neuron of the hidden layer.

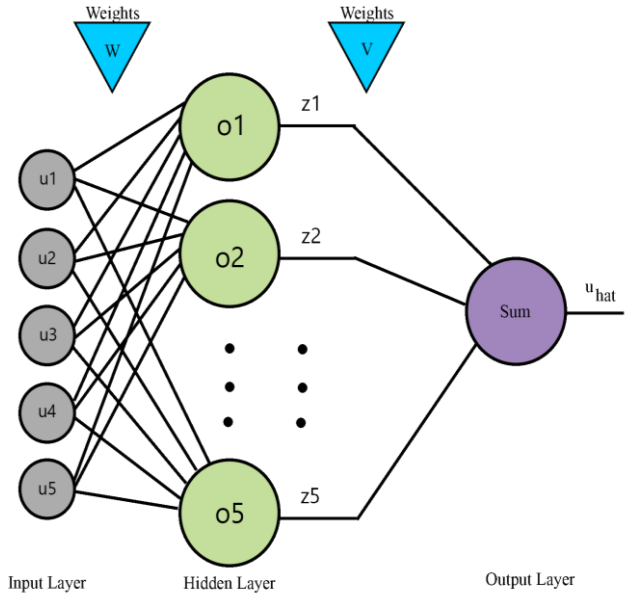

Fig. 4. The structure of the MLP neural network

A nonlinear activation function g(·) is employed in the hidden layer, while a linear activation function f(·) is used in the output layer. The activation functions are defined as follows:

$$\begin{cases} g(x) = \tanh x \\ f(x) = x \end{cases} \quad (15)$$

According to (12), the differential of output temperature and coil current can be expressed by the discrete form as below:

$$\dot{x}_i = \frac{x_i(k+1) - x_i(k)}{T} \quad \forall \ \ i = 1,2 \quad (16)$$

where T is the sample time, $x_1(k)$ is the output temperature of the induction furnace and $x_2(k)$ is the coil current at time step k.

The nonlinear difference equation $D(.)$ between the output temperature y and the input voltage u can be presented as:

$$y(k) = D(u(k), u(k-1), u(k-2), y(k-1), y(k-2)) \quad (17)$$

Thus, the inverse of (17) can be calculated below.

$$u(k) = D^{-1}(u(k-1), u(k-2), y(k), y(k-1), y(k-2)) \quad (18)$$

Using the above difference model, the neural networks shown in Fig. 5, both as the model identifier and the inverse model identifier, have five inputs, five neurons, and one output.

In this section, the system was trained on 800 data points, and 200 points were used for validation.

2) Adaptive Algorithm for Online Learning in MLP

Due to (14) and the structure of the MLP for the desired system, the output of the inverse MLP neural network can be denoted by:

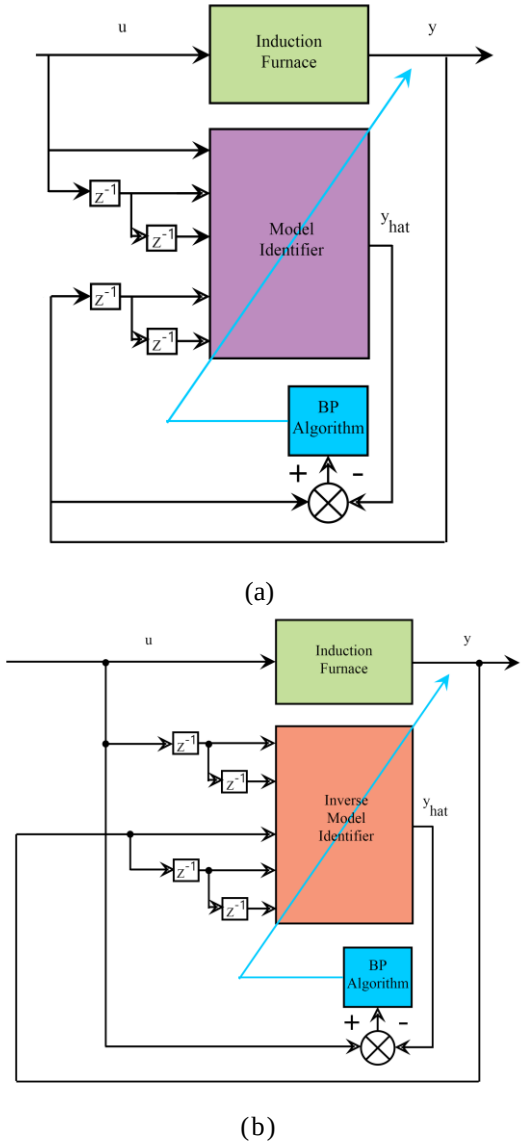

Fig. 5. The block diagram of training using the BP neural network. (a)Model identifier. (b) Inverse model identifier.

$$u_{hat} = V^T \times Z \quad (19)$$

Where V is the weight with dimensions of 5×1 and Z, as the outputs of the hidden layer, can be expressed:

$$Z_{j1} = g(S_{j1}) \qquad , j = 1,2,\cdots,5 \quad (20)$$

S as the inputs of the hidden layer can be shown as follows:

$$S_{j1} = W^T \times U \qquad , j = 1,2,\cdots,5 \quad (21)$$

where the dimension of input weights W is 5×5, and U is the inputs of the MLP neural network.

The gradient descent method and the BP algorithm are applied to update the nonlinear parameters W and V online. The error function I can be expressed below.

$$I^q = \|u^q - {u_{hat}}^q\|^2 , q = 1,2,\cdots,Q \quad (22)$$

Where Q is the number of observations. Consequently, the gradient descent is written as:

$$\begin{cases} w_{ij}^{new} = w_{ij}^{old} - \rho \frac{\partial I^q}{\partial w_{ij}^{old}} \\ i = j = 1,2,\cdots,5 \end{cases} \quad (23)$$

where ρ is the learning rate of the network.

According to (23), the derivative of the error function with respect to the W should be calculated in (24).

$$\frac{\partial I^q}{\partial w_{ij}} = \frac{\partial}{\partial w_{ij}} \|u^q - u_{hat}{}^q\|^2 = -2(u^q - u_{hat}{}^q) \frac{\partial u_{hat}}{\partial w_{ij}} \quad (24)$$

The derivative of the MLP output with respect to the W can be expressed by:

$$\frac{\partial u_{hat}}{\partial w_{i\,j}} = \frac{\partial}{\partial w_{i\,j}} (\sum_{k=1}^{m} Z_k \, v_{k1}) = v_{k1} \frac{\partial Z_k}{\partial w_{i\,j}} \quad (25)$$

So, the derivative of the output neuron with respect to the W can be depicted as:

$$\frac{\partial Z_m}{\partial w_{i\,j}} = \frac{\partial g(S_m)}{\partial w_{i\,j}} \ , m = 1,2,\cdots,5 \quad (26)$$

Now, the chain rule can be used to calculate the above derivative.

$$\frac{\partial g(S_m)}{\partial w_{i\,j}} = \frac{\partial g(S_m)}{\partial S_m} \times \frac{\partial S_m}{\partial w_{i\,j}} = (1 - tanh^2(S_m)) U_m \quad (27)$$

Using (25)-(27), (24) can be rewritten:

$$\frac{\partial I^q}{\partial w_{ij}} = -2(u^q - u_{hat}{}^q) v_{k1} U_k (1 - tanh^2(S_k)) \quad (28)$$

Due to (28), (23) can be reconstructed as:

$$w_{ij}^{new} = w_{ij}^{old} + \rho 2(u^q - u_{hat}{}^q) v_{k1} U_k (1 - tanh^2(S_k)) \quad (29)$$

In the next step, V parameters can be adjusted using the gradient descent method.

The error function I is proposed by:

$$I^q = \|u^q - u_{hat}{}^q\|^2 \ , q = 1,2,\cdots,Q \quad (30)$$

Using the gradient descent, the update rules are shown as:

$$\begin{cases} v_{ij}^{new} = v_{ij}^{old} - \rho \frac{\partial I^q}{\partial v_{ij}^{old}} \\ i = j = 1,2,\cdots,5 \end{cases} \quad (31)$$

The derivative of the error function with respect to the V weight can be reestablished.

$$\frac{\partial I^q}{\partial v_{i1}} = \frac{\partial}{\partial v_{i1}} \|u^q - u_{hat}{}^q\|^2 = -2(u^q - u_{hat}{}^q) \frac{\partial u_{hat}}{\partial v_{i1}} \quad (32)$$

$\frac{\partial u_{hat}}{\partial v_{i1}}$ can be determined as follows:

$$\begin{cases} \frac{\partial u_{hat}}{\partial v_{i\,1}} = \frac{\partial}{\partial v_{i\,1}} (\sum_{k=1}^{m} Z_{k1} \, v_{k1}) = Z_m \\ m = 1,2,\cdots,5 \end{cases} \quad (33)$$

By (32) and (33), the update rules of V are as:

$$v_{ij}^{new} = v_{ij}^{old} + \rho 2(u^q - u_{hat}{}^q) Z_m \quad (34)$$

C. MLP ALGORITHM:

The design procedure of the MLP-based inverse model is summarized as follows:

Step 1: Online inverse model identification
Construct the MLP neural network structure as defined in (19).

Step 2: Online weight adaptation using the BP algorithm
Define the error function according to (22) and incorporate it into the gradient descent formulation given in (23). Based on (22) and (23), the weight update laws in (29) and (34) are derived and applied.

Step 3: Weight transfer to the controller
The updated weights are transferred to the inverse model controller, which has the same structure as the inverse model identifier.

Step 4: Iterative adaptation
Repeat Step 2 and Step 3 continuously during online operation.

IV. ADAPTIVE INVERSE ANFIS CONTROLLER

The ANFIS model structure was carefully selected to balance modeling accuracy and computational efficiency, particularly under online learning conditions. Each input variable was assigned five Gaussian membership functions, which were found to provide sufficient nonlinear representation capability without causing excessive rule explosion. Gaussian membership functions were chosen due to their smoothness, continuous differentiability, and robustness in gradient-based adaptive algorithms. The fuzzy rule base was automatically generated using a first-order Takagi–Sugeno–Kang (TSK) inference mechanism. This approach eliminates subjective manual rule design and ensures that the rule structure is systematically derived from the input space partitioning. As a result, the number of rules is directly related to the number of membership functions per input, allowing consistent model scalability.

This section presents the ANFIS model and both the Model identifier and the Inverse model identifier. The ANFIS includes features of fuzzy systems and artificial neural networks. The ANFIS structure has five layers, as shown in Fig. 6: Layer 1: fuzzification layer with adaptive nodes; Layer 2: product layer; Layer 3: normalized layer; Layer 4: defuzzification layer; and Layer 5: output layer.

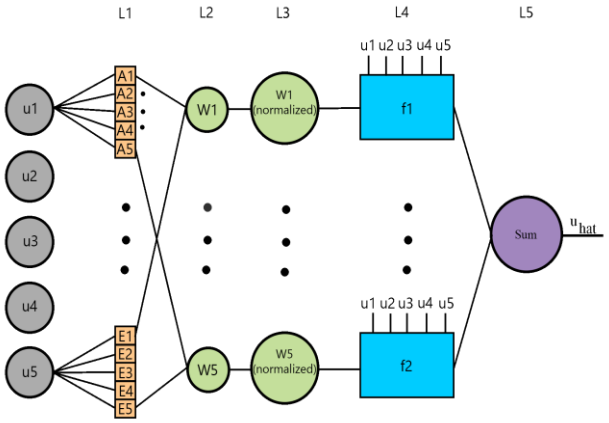

Fig. 6. The structure of the ANFIS neural network

In the first layer, five membership functions $(A_i, B_i, C_i, D_i, E_i)$ are used for each input. The second layer normalized fuzzy inputs for the third layer. The task of the fourth layer is defuzzification of the output of the third layer. The last layer is an aggregation layer.

$$A = \frac{1}{1+(\frac{u_i - c_j}{a_j})^{2b_j}} \tag{35}$$

where a, b, and c are called the premise parameters, and i and j =1,2,3,4,5.

So, the output of the first layer can be written as:

$$O_{1,i} = A(u_i) \tag{36}$$

The output of the second one, which is called the firing strength of the rule, is calculated as follows.

$$O_{2,i} = W_i = A_i B_i C_i D_i E_i \tag{37}$$

Now, in the third layer, the firing strength of each rule is normalized using (38).

$$O_{3,i} = \bar{W}_i = \frac{W_i}{\sum_{k=1}^{5} W_k} \tag{38}$$

The TSK (Takagi Sugeno Kang) inference method is used for fuzzy rule bases. Hence, it can be written:

$$f_i = p_i u_1 + q_i u_2 + r_i u_3 + s_i u_4 + t_i u_5 + z_i \tag{39}$$

where p, q, r, s, t, z are called consequent parameters. The outputs of adaptive nodes in the fourth layer are given by:

$$O_{4,i} = \bar{W}_i f_i \tag{40}$$

In conclusion, the output of the last layer is:

$$O_{5,i} = \sum_{k=1}^{5} \bar{W}_i f_i \tag{41}$$

A. Adaptive Algorithm for Online Learning in ANFIS

In ANFIS, consequent and premise parameters must be updated adaptively. Hence, in the first step, the error function is expressed by:

$$I^q = \|u^q - {u_{hat}}^q\|^2 , q = 1,2,\cdots,Q \tag{42}$$

The gradient descent method to update premise parameters θ is derived as:

$$\theta_{ij}^{new} = \theta_{ij}^{old} - \rho \frac{\partial I^q}{\partial \theta_{ij}^{old}} \tag{43}$$

For calculation $\frac{\partial I^q}{\partial \theta_{ij}^{old}}$, the following derivative chain can be constructed:

$$\begin{cases} \frac{\partial I^q}{\partial \theta_{ij}} = \frac{\partial I^q}{\partial O_5}\frac{\partial O_5}{\partial O_4}\frac{\partial O_4}{\partial O_3}\frac{\partial O_3}{\partial O_2}\frac{\partial O_2}{\partial O_1}\frac{\partial O_1}{\partial \theta_{ij}} \\ \frac{\partial I^q}{\partial O_5} = -(u^q - {u_{hat}}^q) \\ \frac{\partial O_5}{\partial O_4} = 1 \\ \frac{\partial O_4}{\partial O_3} = f_i \\ \frac{\partial O_3}{\partial O_2} = \frac{\sum_{k=1}^{5} W_k - W_i}{(\sum_{k=1}^{5} W_k)^2} \\ \frac{\partial O_2}{\partial O_1} = \sum_{k=1}^{5} \sum_{l=1}^{5} A_{kl} B_{kl} C_{kl} D_{kl} E_{kl} \end{cases} \tag{44}$$

Using (44), three premise parameters for $\frac{\partial O_1}{\partial \theta_{ij}}$ can be expressed below:

$$\begin{cases} \frac{\partial O_1}{\partial a_{ij}} = \frac{2b_{ij}(c_{ij}-u_i)^2}{a_{ij}^3(\frac{b_{ij}(c_{ij}-u_i)^2}{a_{ij}^2+1})^2} \\ \frac{\partial O_1}{\partial b_{ij}} = \frac{-(c_{ij}-u_i)^2}{a_{ij}^2(\frac{b_{ij}(c_{ij}-u_i)^2}{a_{ij}^2+1})^2} \\ \frac{\partial O_1}{\partial c_{ij}} = \frac{-2b_{ij}(c_{ij}-u_i)}{a_{ij}^2(\frac{b_{ij}(c_{ij}-u_i)^2}{a_{ij}^2+1})^2} \end{cases} \tag{45}$$

premise parameters used in the membership function, and the membership degree of each function is calculated by using the premise parameter set.

Using membership function properties, and according to (44), (46) can be rewritten:

$$\begin{cases} \frac{\partial I^q}{\partial a_{ij}} = -(u^q - {u_{hat}}^q) f_i \frac{\sum_{k=1}^{5} W_k - W_i}{(\sum_{k=1}^{5} W_k)^2} \sum_{k=1}^{5} \sum_{l=1}^{5} A_{kl} B_{kl} C_{kl} D_{kl} E_{kl} \frac{2b_{ij}(c_{ij}-u_i)^2}{a_{ij}^3(\frac{b_{ij}(c_{ij}-u_i)^2}{a_{ij}^2+1})^2} \\ \frac{\partial I^q}{\partial b_{ij}} = -(u^q - {u_{hat}}^q) f_i \frac{\sum_{k=1}^{5} W_k - W_i}{(\sum_{k=1}^{5} W_k)^2} \sum_{k=1}^{5} \sum_{l=1}^{5} A_{kl} B_{kl} C_{kl} D_{kl} E_{kl} \frac{-(c_{ij}-u_i)^2}{a_{ij}^2(\frac{b_{ij}(c_{ij}-u_i)^2}{a_{ij}^2+1})^2} \\ \frac{\partial I^q}{\partial c_{ij}} = -(u^q - {u_{hat}}^q) f_i \frac{\sum_{k=1}^{5} W_k - W_i}{(\sum_{k=1}^{5} W_k)^2} \sum_{k=1}^{5} \sum_{l=1}^{5} A_{kl} B_{kl} C_{kl} D_{kl} E_{kl} \frac{-2b_{ij}(c_{ij}-u_i)}{a_{ij}^2(\frac{b_{ij}(c_{ij}-u_i)^2}{a_{ij}^2+1})^2} \end{cases} \tag{46}$$

Now, the gradient descent method is applied to update the consequent parameter φ as below.

$$\begin{cases} \frac{\partial I^q}{\partial \varphi_{ij}} = \frac{\partial I^q}{\partial O_5}\frac{\partial O_5}{\partial O_4}\frac{\partial O_4}{\partial \varphi_{ij}} \\ \frac{\partial I^q}{\partial O_5} = -(u^q - {u_{hat}}^q) \\ \frac{\partial O_5}{\partial O_4} = 1 \end{cases} \tag{47}$$

As the existence of the six consequent parameters, then for $\frac{\partial O_1}{\partial \varphi_{ij}}$ should be expressed:

$$\begin{cases} \frac{\partial O_4}{\partial p_i} = \bar{W}_i u_1 \\ \frac{\partial O_4}{\partial q_i} = \bar{W}_i u_2 \\ \frac{\partial O_4}{\partial r_i} = \bar{W}_i u_3 \\ \frac{\partial O_4}{\partial s_i} = \bar{W}_i u_4 \\ \frac{\partial O_4}{\partial t_i} = \bar{W}_i u_5 \\ \frac{\partial O_4}{\partial z_i} = \bar{W}_i \end{cases} \quad (48)$$

According to (47), (48) can be depicted as:

$$\begin{cases} \frac{\partial I^q}{\partial p_i} = -(u^q - u_{hat}{}^q)\bar{W}_i u_1 \\ \frac{\partial I^q}{\partial q_i} = -(u^q - u_{hat}{}^q)\bar{W}_i u_2 \\ \frac{\partial I^q}{\partial r_i} = -(u^q - u_{hat}{}^q)\bar{W}_i u_3 \\ \frac{\partial I^q}{\partial s_i} = -(u^q - u_{hat}{}^q)\bar{W}_i u_4 \\ \frac{\partial I^q}{\partial t_i} = -(u^q - u_{hat}{}^q)\bar{W}_i u_5 \\ \frac{\partial I^q}{\partial z_i} = -(u^q - u_{hat}{}^q)\bar{W}_i \\ i = 1,2,\cdots,5 \quad , q = 1,2,\cdots,Q \end{cases} \quad (49)$$

B. ANFIS ALGORITHM:

The design procedure of the ANFIS-based inverse model is summarized as follows:

Step 1: Online inverse model identification
Construct the ANFIS structure according to (36)–(41).

Step 2: Online parameter adaptation
Define the error function as given in (42) and incorporate it into the gradient descent formulation in (43). Based on this formulation, the premise parameters and consequent parameters are updated using (46) and (49), respectively.

Step 3: Parameter transfer to the inverse controller
The updated parameters are transferred to the inverse model controller, which has the same structure as the inverse model identifier.

Step 4: Iterative adaptation
Repeat Step 2 and Step 3 continuously during online operation.

V. SIMULATION RESULTS

In this section, all the proposed methods presented in the previous sections are applied to the nonlinear model of the induction furnace. The induction furnace needs to operate at the desired temperature required to melt the material. In this case, the desired temperature is considered as 912 °C, which is suitable for producing iron ferrite products with a carbon content of 12.22 wt%. The induction furnace parameters are shown in Table I [3].

A. Fault Modeling Strategy and Practical Relevance

In this study, input faults are modeled as multiplicative disturbances applied over finite time intervals. Specifically, fault conditions are introduced during the sample intervals 200–300 and 400–500, emulating sustained actuator degradation, voltage drop, or power electronics uncertainty that typically persists for a certain duration in industrial induction furnace systems. Modeling faults over time intervals enables the assessment of the controller's ability to maintain tracking performance under prolonged abnormal operating conditions, as well as its capacity for re-adaptation after fault clearance. Although the fault magnitudes and occurrence intervals are predefined, this approach provides a reproducible and meaningful benchmark for evaluating the fault-tolerant characteristics of the proposed adaptive inverse control structure. The scope of fault tolerance demonstrated in this work is therefore limited to a representative class of sustained input faults and should be interpreted accordingly.

Case 1: Simulation results of MLP Network

The proposed model and inverse model identifier based on the MLP neural network are discussed in this case. The sampling time is chosen 0.01 *sec* with the learning rate of 0.03. The fault in the system's input is considered multiplicative, with a range of $\pm 10\%$.

TABLE I
Induction Furnace Parameters [3]

Parameters	Value
L_{eq}	$7.2211 \times 10^{-4}\ H$
R_{eq}	$4.81 \times 10^{-2}\ \Omega$
m	$500\ kg$
c	$450\ J/kg\ oC$
J_1	38.5347
k_{pwg}	28.02
k_G	0.267
y_c	0−15 V
V_{dc}	140.115

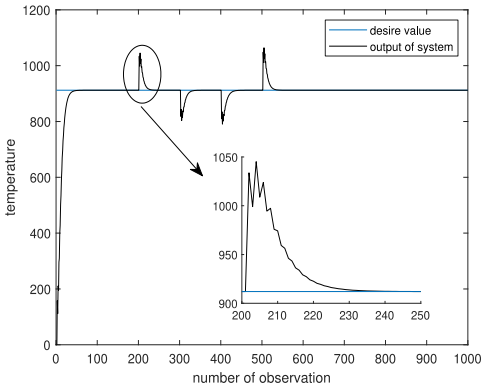

Fig. 7. The simulation results for tracking the desired temperature with the MLP neural network

As shown in Fig. 7, AIDC with the MLP neural network can dampen the fault's effects on the system's output that occur at 200-300, and 400-500 samples. Fig. 8 shows the control signal and the effect of the faults in the control input to fix the faults.

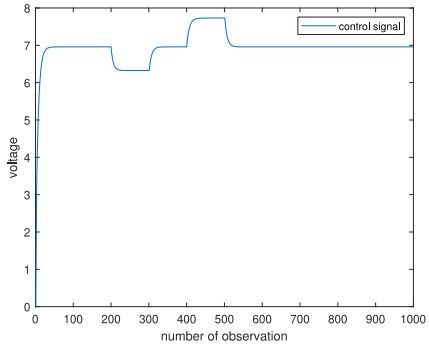

Fig. 8. The control signal of AIDC with MLP neural network

The error between the desired output and the AIDC output is shown in Fig. 9.

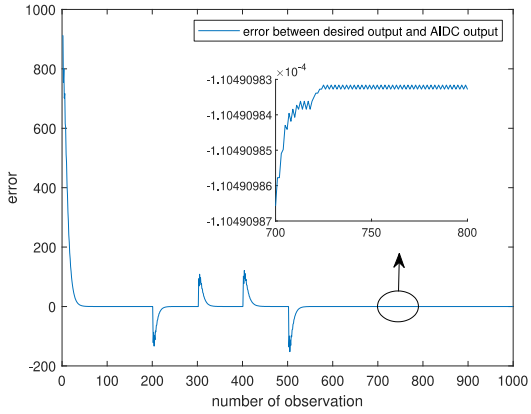

Fig. 9. The error of AIDC with the MLP neural network

The accuracy of performance or error between the AIDC output and the desired output in this method is in the order of 10^{-4}, which is considered acceptable accuracy.

Case 2: Simulation results of ANFIS Network

The proposed model and inverse model identifier based on the ANFIS Network are discussed in this approach. Likewise, the sampling time is chosen 0.01 *sec* with the learning rate of 0.03. The fault in the input of the system is considered multiplicative with a range of $\pm 10\%$. The AIDC with ANFIS can reduce fault effects that occur in 200-300, and 400-500 samples.

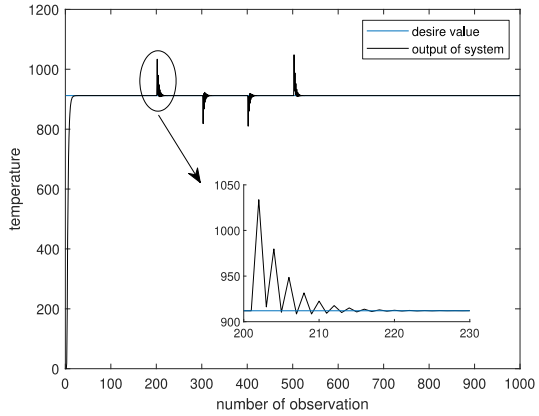

Fig. 10. The simulation results for tracking the desired temperature with the ANFIS neural network

Fig. 10 shows that the system can reduce the fault effect with an acceptable accuracy of 10^{-5}.

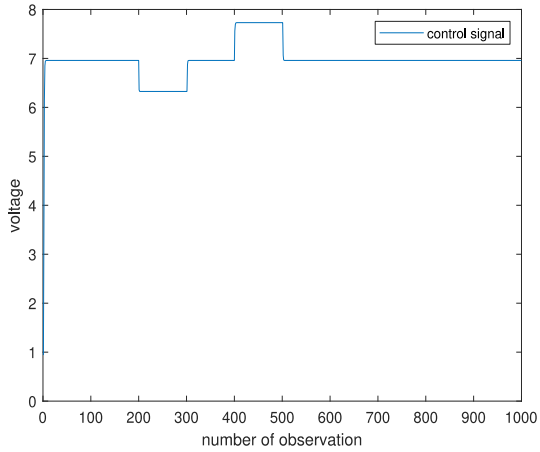

Fig. 11. The control signal of AIDC with ANFIS neural network

The control input signal is shown in Fig. 11.

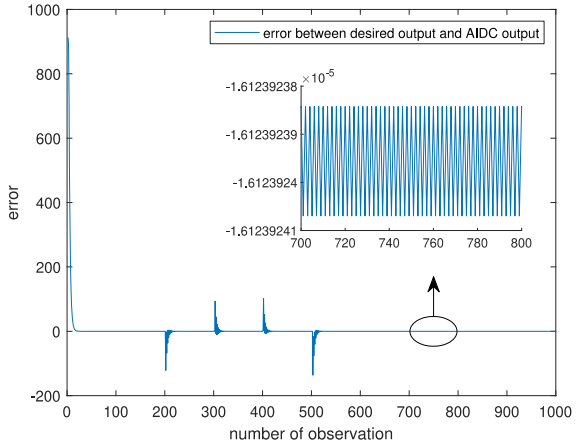

Fig. 12. The error of AIDC with the ANFIS neural network

As shown in this section, it is evident that the AIDC with ANFIS performs better than the MLP network in handling the input faults. To provide an objective comparison between the MLP-based and ANFIS-based AIDC approaches, standard quantitative indicators were evaluated. The RMS tracking error was calculated over samples k≥70 to exclude the initial transient response. The RMS error equals 1.2302 for the MLP-based method and 0.5025 for the ANFIS-based method, confirming a lower average tracking error for ANFIS.

VI. ADAPTIVE INVERSE CONTROLLER

The neural network structures were not selected arbitrarily. To enable a fair comparison between the MLP- and ANFIS-based controllers, both models were designed under identical conditions, including the same input signals and delay structure. In the ANFIS framework, increasing the number of membership functions beyond five per input results in exponential growth in the number of fuzzy rules, leading to excessive computational complexity that is undesirable for adaptive control applications. Therefore, the network size was deliberately limited to balance approximation capability and practical implementation. Regarding input delays, a single delay was insufficient to capture the system dynamics, while more than two delays significantly increased model complexity and overfitting risk without noticeable performance improvement. Consequently, two input delays were selected as a practical compromise. The MLP architecture was chosen with a single hidden layer, which is well known to be sufficient for approximating nonlinear

system dynamics while preserving computational efficiency and stability in adaptive control implementations.

In neural-network-based adaptive control with online backpropagation, providing a rigorous closed-loop stability proof is generally challenging due to the nonlinear and time-varying learning dynamics and the coupling between the plant and the adaptation law. Therefore, the learning rate is chosen to be sufficiently small, and the network structure is kept compact to limit parameter fluctuations. In this work, the objective of adaptation is to ensure bounded parameter evolution and satisfactory tracking performance rather than strict weight convergence.

The learning rate and sampling time were conservatively selected to ensure bounded weight updates and smooth control action. Throughout all simulation scenarios, including prolonged fault intervals and repeated disturbances, the controller exhibited stable behavior without divergence or oscillatory response. Therefore, the stability and robustness claims of this work should be interpreted in terms of empirical performance preservation and practical stability under reasonable parameter settings.

VII. CONCLUSION

This paper investigates inverse dynamic procedures using both MLP and ANFIS to track the desired temperature trajectory in an induction furnace while mitigating input faults. The BP algorithm was employed for adaptive parameter updates in both methods, demonstrating fault tolerance and satisfactory accuracy in reaching the target temperature. Simulation results indicate that the ANFIS network outperforms the MLP, requiring approximately 20 samples to effectively manage faults without overshooting or undershooting, compared to 40 for the MLP. Additionally, ANFIS achieves the desired temperature more quickly than MLP. Moreover, after fault removal, the maximum residual tracking error is approximately $1.1\times10-4$ for MLP and $1.61\times10-5$ for ANFIS, demonstrating a significantly reduced steady-state error with the ANFIS-based controller. These quantitative results support the improved tracking performance of ANFIS under the considered scenarios. RMS error inherently captures fault-induced transients and therefore should be interpreted as a fault-inclusive performance indicator rather than a pure steady-state metric. Future work may explore deep learning applications in both methodologies and implement these strategies in real induction furnaces.

FUNDING

The authors received no specific funding for this work.

CONFLICTS OF INTEREST/COMPETING INTERESTS

The authors declare that they have no conflict of interest.

AVAILABILITY OF DATA AND MATERIAL

There is no data for availability.

CODE AVAILABILITY

All the MATLAB codes are attached to journal.

AUTHORS' CONTRIBUTIONS

Alireza Borjali, Reza Ghasemi deal with Substantial contributions to the conception or design of the work; or the acquisition, analysis, or interpretation of data for the work, Drafting the work or reviewing it critically for important intellectual content; Final approval of the version to be published, Agreement to be accountable for all aspects of the work in ensuring that questions related to the accuracy or integrity of any part of the work are appropriately investigated and resolved.

ACKNOWLEDGMENTS

The authors gratefully acknowledge the support for this work provided by the University of Qom.

REFERENCES

[1] S. V. B., A. B. Vivek R. Gandhewar, "Induction Furnace - A Review," International Journal of Engineering and Technology, vol. 3, no. 4, pp.277-284, 2011.

[2] P. Tawdee, "An Induction Furnace Employing with Half Bridge Series Resonant Inverter," IEEE, vol. 4, no. 3, p. 3, 2014.

[3] A. S.-R. P. H. R. Rina Ristiana, "Modeling and Control of Temperature Dynamics In Induction Furnace System," IEEE 5th International Conference on System Engineering and Technology, pp. 6-11, 2015.

[4] J. C. Tudon-Martinez, J. de-J. Lozoya-Santos, A. Cantu-Perez, and A. Cardenas-Romero, “Advanced temperature control applied on an industrial box furnace,” Journal of Thermal Science and Engineering Applications, vol. 14, no. 6, Art. no. 061001, Jun. 2022, doi: 10.1115/1.4052020.

[5] Y. Hu, C. K. Tan, J. Broughton, P. A. Roach, and L. Varga, “Nonlinear dynamic simulation and control of large-scale reheating furnace operations using a zone method-based model,” Applied Thermal Engineering, vol. 135, pp. 156–176, 2018, doi: 10.1016/j.applthermaleng.2018.02.022. [6] M. R. O. J. S. Ordoñez Rafael, "Simulation of a Temperature Fuzzy Control into Induction Furnace," IEEE, 2016 13th International Conference on Power Electronics (CIEP), pp. 64-69, 2016.

[6] M. R. O. J. S. Ordoñez Rafael, "Simulation of a Temperature Fuzzy Control into Induction Furnace," IEEE, 2016 13th International Conference on Power Electronics (CIEP), pp. 64-69, 2016.

[7] A. K. F. Roetzer ∗ A. Aschauer ∗ L. Jadachowski ∗∗ A. Steinboeck ∗, "Temperature Control for Induction Heating of thin strips," ScienceDirect, vol. 53, no. 2, pp. 11968-11973, 2020.

[8] A. Tepljakov, E. Petlenkov, and J. Belikov, “Fractional-order PID controllers in temperature control applications: A review,” Energies, vol. 15, no. 11, Art. no. 3800, 2022.

[9] J. Hu, J. Cai, and Y. Li, “Distributed adaptive temperature control for multi-zone HVAC systems with inter-zone thermal coupling,” Energy and Buildings, vol. 199, pp. 25–38, 2020. [12] W. W. Y. W. C. S. a. Q. C. Xuanyu Liu1, "Coordinated optimization control of shield machine based on dynamic fuzzy neural network direct inverse control," Sage Journals, Transactions of the Institute of Measurement and Control, vol. 43, no. 6, pp. 1445–1451, 2021.

[10] W.-H. Zuo, B.-C. Liu, and W.-J. Zhu, “An improvement of decoupling control research of gas heating furnace temperature system,” in Proc. IEEE Int. Conf. on Control and Automation, 2015, pp. 102–106, doi: 10.1109/ICCA.2015.7320000.

[11] A. Bublikov, M. Isakova, V. Nadtochyi, D. Zybalov, Yu. Halchenko, and M. Khoroshailov, “Modified algorithm of automatic temperature control in an electric resistance furnace for metal heat treatment,” Automation and Computer-Integrated Technologies, vol. 70, pp. 134–145, 2021, doi: 10.33271/crpnmu/70.134.

[12] A. S. O. O. I. Okafor P.U., "Artificial Neural Network Inverse Model (AIM) Based Position Control Of DC Motor," International Journal of Engineering, Science and Mathematics, vol. 9, no. 2, pp. 77-84, 2020.

[13] M. B. Errachdi Ayachi, "Adaptive Internal Model Neural Networks Control for Nonlinear System," Researchgate journals, Proceedings of the 2013 International Conference on Systems, Control and Informatics, pp. 78-83, 2013.

[14] Y. L. a. S. T. Wei Wu, "Fuzzy Adaptive Tracking Control for State Constraint Switched Stochastic Nonlinear Systems With Unstable Inverse Dynamics," IEEE, vol. 51, no. 9, pp. 5522 - 5534, 2019.

[15] K. S. A. A. S. M. S. Mojtaba Kordestani, "An Adaptive Passive Fault Tolerant Control System for a Steam Turbine Using a PCA Based Inverse Neural Network Control Strategy," IEEE, 2018 World Automation Congress (WAC), pp. 40-45, 2018.

[16] D. S. H. a. D. R. L. Carlos Robles Algarín *, "A Low-Cost Maximum Power Point Tracking System Based on Neural Network Inverse Model Controller," Electronics, vol. 7, no. 1, p. 17, 2018.

[17] W. P. W. Z. Q. W. S. F. H. D. a. F. L. Youqun Zhao*, "A Vehicle Handling Inverse Dynamics Method for Emergency Avoidance Path Tracking Based on Adaptive Inverse Control," IEEE, p. 13, 2021.

[18] S. P. •. G. Panda, "Performance Evaluation of a New BP Algorithm for a Modified Artificial Neural Network," Springer, pp.1869-1889, 2020.

[19] W. W. a. B. K. M Ary Heryanto, "Optimization of a neural network based direct inverse control for controlling a quadrotor unmanned aerial vehicle," International Conference on Mechatronics and Mechanical Engineering (ICMME 2015), EDP Sciences, vol. 34, pp. 1-4, 2015.

[20] B. K. Afrias Sarotama, "Position Difference for System Identification and Control of UAV Alap-Alap Using Back Propagation Algorithm Neural Network with Kalman Filter," American Journal of Intelligent Systems, vol. 5, no. 1, pp.18-26, 2015.

[21] W. W. Y. W. C. S. a. Q. C. Xuanyu Liu1, "Coordinated optimization control of shield machine based on dynamic fuzzy neural network direct inverse control," Sage Journals, Transactions of the Institute of Measurement and Control, vol. 43, no. 6, pp. 1445–1451, 2021.

[22] M. M. a. A. M. E.-S. M. M. Ahmed, "Design of a Coreless Induction Furnace for Melting Iron," INTERNATIONAL CONFERENCE ON COMMUNICATION, COMPUTER AND POWER (ICCCP'09), pp. pp. 102-106, 2009.